In vivo quantification of pulmonary inflammation in relation to emphysema severity via partial volume corrected ^{18}F-FDG-PET using computer-assisted analysis of diagnostic chest CT

Drew A. Torigian[1*] MD, MA,
Vincent Dam[1*] MD,
Xinjian Chen[2] PhD,
Babak Saboury[1] MD, MPH,
Jayaram K. Udupa[1] PhD,
Arif Rashid[1] BA,
Siamak Moghadam-Kia[1] MD,
Abass Alavi[1] MD, MD (Hon.), PhD (Hon.), DSc (Hon.)
(*Please note, the first two authors have contributed equally to this manuscript.)

1. Department of Radiology, Hospital of the University of Pennsylvania, Philadelphia, PA, USA
2. School of Electronics and Information Engineering, Soochow University, China

***

Keywords: Inflammation - Emphysema - COPD - ^{18}F-FDG-PET - PET/CT quantification

Correspondence address:
Drew A. Torigian, MD, MA
Department of Radiology
Hospital of the University of Pennsylvania, 3400 Spruce Street, Philadelphia, PA 19104
Phone: 215-615-3805
Fax: 215-614-0033
Email: Drew.Torigian@uphs.upenn.edu

Received:
18 September 2012
Accepted:
16 October 2012

Abstract

Our aim was to quantify the degree of pulmonary inflammation associated with centrilobular emphysema using fluoro-18-2-fluoro-2-deoxy-D-glucose positron emission tomography (^{18}F-FDG-PET) and diagnostic unenhanced computed tomography (CT) based image segmentation and partial volume correction. *Forty-nine subjects*, with variable amounts of centrilobular emphysema, who had prior diagnostic unenhanced chest CT and either ^{18}F-FDG-PET or ^{18}F-FDG-PET/CT were selected. Lung parenchymal volume (L) (in cm^3) excluding large and small pulmonary vessels, emphysema volume (E) (in cm^3) based on a -910HU threshold, fraction of lung emphysema (F=E/L), and mean attenuation (HU) of non-emphysematous lung parenchyma (A) were calculated from CT images using the image analysis software 3DVIEWNIX. Lung uncorrected maximum SUV (USUVmax) was measured manually from PET images on a dedicated workstation. A first level of partial volume correction (PVC) of lung SUVmax to account for presence and degree of macroscopic emphysematous air space was calculated as CSUVmax=USUVmax/(1-F). A second level of PVC of non-emphysematous lung SUVmax to account for the mixture of air and lung parenchyma at the microscopic level was then estimated as CCSUVmax=CSUVmax/(A+1000/1040), assuming that air is -1000HU in attenuation and gasless lung parenchyma is 40HU in attenuation. The correlation of F with USUVmax, CSUVmax, CCSUVmax, % change between CSUVmax and USUVmax (%UC), and % change between CCSUVmax and USUVmax (%UCC) were then tested. *The results showed* that USUVmax was not significantly correlated with F (r=-.0973, P=0.34). CSUVmax (r=0.4660, P<0.0001) and CCSUVmax were significantly positively correlated with F (r=0.5479, P<0.0001), as were %UC (r=0.9383, P<0.0001) and %UCC (r=0.9369, P<0.0001). *In conclusion*, the degree of pulmonary inflammation increases with emphysema severity based on ^{18}F-FDG-PET or ^{18}F-FDG-PET/CT assessment, but is only detectable when ^{18}F-FDG uptake is corrected for the partial volume effect based on data provided from diagnostic chest CT images. These results support the notion that pulmonary inflammation plays an important role in the pathophysiology of emphysema. This novel image analysis approach has great potential for practical, accurate, and precise combined structural-functional PET quantification of pulmonary inflammation in patients with emphysema or other pulmonary conditions, although further validation and refinement will be required.

Hell J Nucl Med 2013; 16(1): 12-18 *Epub ahead of print: 26-3-2013* *Published on line: 10 April 2013*

Introduction

Chronic obstructive pulmonary disease (COPD), a complex multifactorial multiphenotypic disease condition characterized by chronic airflow obstruction (due to emphysema and/or small airways disease), is a major cause of morbidity and mortality worldwide. It is the 3rd leading cause of death in the United States, and is the only leading cause that is increasing in prevalence. By 2030, it is estimated that nearly 9 million people will die each year from COPD. Furthermore, the associated health care costs are enormous [1-3]. A large number of potential biomarkers for purposes of COPD risk assessment, phenotype identification, and diagnosis of exacerbation have already been assessed, including imaging-based biomarkers obtained from computed tomography (CT) and hyperpolarized gas magnetic resonance imaging (MRI), although their performance is quite variable such that no single biomarker in COPD warrants wide acceptance [4] at present. As such, there is still a need for molecular, physiological, and imaging-based biomarkers in COPD that can be used both in identifying specific COPD phenotypes and as surrogate endpoints in clinical trials [5-7].

Fluoro-18-2-fluoro-2-deoxy-D-glucose positron emission tomography (^{18}F-FDG-PET) is a non-invasive quantitative molecular imaging technique that has increasingly been utilized to quantify pulmonary and airways inflammation in both animal studies and human studies. As such, it has the potential to play an important role in the quantitative assessment

of patients with COPD for purposes of individualized disease phenotyping, pretreatment planning, disease course prediction, outcome prognostication, and response assessment, as inflammation is a key contributor to the development and progression of COPD. However, ^{18}F-FDG-PET has been underutilized for the assessment of patients with COPD.

Therefore, the aim of this preliminary study was to quantify the relationship of the degree of pulmonary parenchymal inflammation with the degree of centrilobular emphysema using ^{18}F-FDG-PET or ^{18}F-FDG-PET/CT in conjunction with diagnostic CT based image segmentation and partial volume correction.

Materials and methods

Study sample

Following IRB approval for retrospective data collection and image analysis along with HIPAA waiver prior to study initiation, we conducted a retrospective search for subjects with variable amounts of centrilobular emphysema who had prior diagnostic unenhanced chest CT and either ^{18}F-FDG-PET or ^{18}F-FDG-PET/CT imaging without intervening therapy. Forty nine subjects total (35 men and 14 women, age range 41-79 years) with variable amounts of centrilobular emphysema (12 none, 13 mild, 13 moderate, and 11 severe based on qualitative visual assessment) and either ^{18}F-FDG-PET (12 total) or ^{18}F-FDG-PET/CT (37 total) were included in this study. Twenty two had a history of prior malignancy whereas the remaining 27 did not. The average interval time between diagnostic CT and ^{18}F-FDG-PET or ^{18}F-FDG-PET/CT scan acquisition was 39 days (range 0-139 days). A total of 98 individual lungs (2 from each subject) were thus evaluated overall for the purposes of this study.

Chest CT image acquisition

Routine diagnostic quality unenhanced chest CT examinations were acquired on 16 or 64 multidetector row CT scanners (Siemens Medical Solutions, Malvern, PA) during a full inspiratory breathold using a slice collimation of 16x0.75mm or 64x0.6mm**,** respectively, a kVp of 120, an average effective tube current-time product of 200mAs, with tube current modulation on, and a gantry rotation time of 0.5sec. Images were typically reconstructed at a nominal slice thickness of 5mm with an interval of 5mm, a 512x512 matrix, and a B50f reconstruction kernel. Computed tomography images were viewed using dedicated image visualization and analysis software (Terarecon Inc., San Mateo, CA, USA).

PET and PET/CT image acquisition

All subjects fasted for at least 4h prior to PET or PET/CT scanning and, shortly before the injection of the ^{18}F-FDG radiotracer, received fingerstick blood glucose measurements to ensure that serum glucose levels were <150mg/dL at the time of radiotracer injection. Routine ^{18}F-FDG-PET examinations were performed using a dedicated whole-body scanner (Allegro, Philips Medical Systems, Bothell, WA), and routine ^{18}F-FDG-PET/CT scans were acquired using a 16 detector-row LYSO whole-body PET/CT scanner with time-of-flight capabilities (Gemini TF, Philips Medical Systems, Bothell, WA). 3D PET data were acquired from the skull base to mid thighs 60min after intravenous administration of ~555MBq of ^{18}F-FDG for 3min per bed position. For PET only scans, images were reconstructed at 5mm nominal slice thickness using an iterative ordered-subset expectation maximization algorithm with 4 iterations and 8 subsets, and transmission scans using a cesium-137 (^{137}Cs) point source were interleaved between emission scans to correct for non-uniform attenuation. For PET/CT scans, image reconstruction was performed at 5mm nominal slice thickness using a list-mode maximum-likelihood expectation-maximization (ML-EM) algorithm with 33 ordered subsets and 3 iterations, and the system model included time-of-flight as well as normalization, attenuation, randoms, and scatter corrections, where rescaled low-dose

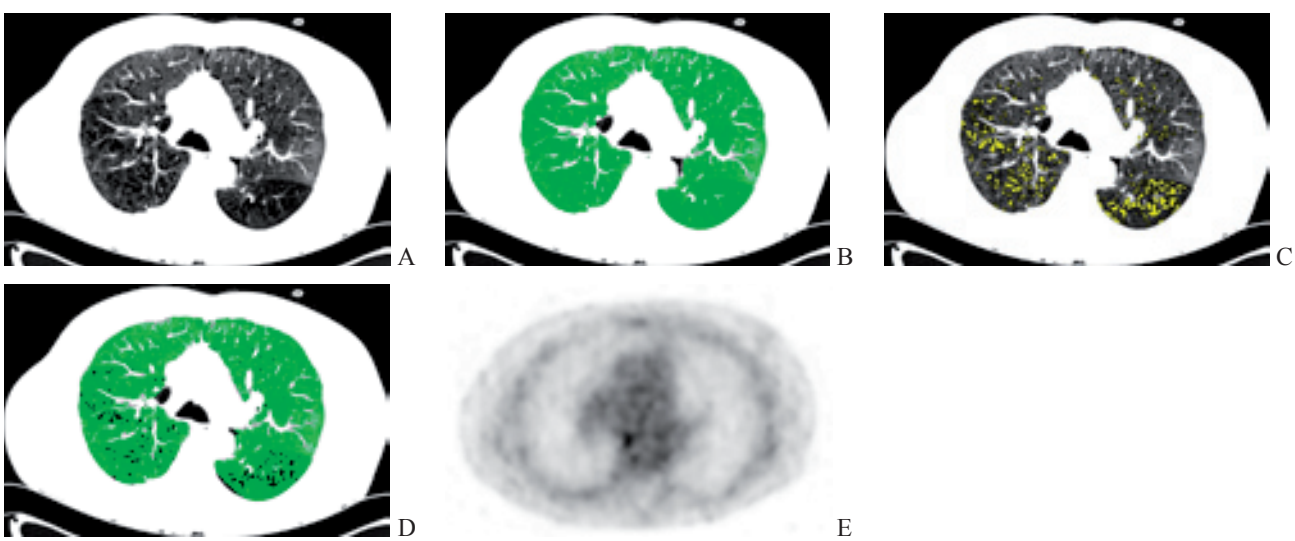

Figure 1. A 66 years old man with centrilobular emphysema. A. Axial chest CT image reveals mild centrilobular emphysema in upper lung zones. B. Same axial chest CT image with color overlay demonstrates bilateral lung segmentation with exclusion of pulmonary vessels. C. Same axial chest CT image with new color overlay highlights voxels with attenuation $\leq$ -910HU in lungs considered as emphysematous. D. Same axial chest CT image with new color overlay shows remaining voxels in lungs considered as non-emphysematous. E. Corresponding axial ^{18}F-FDG-PET image through upper lung zones shows similar degree of ^{18}F-FDG uptake in right and left lungs at this level.

CT images were utilized for attenuation correction of PET images. Attenuation-corrected images from PET and PET/CT only were utilized for purposes of SUV measurement in this study.

Chest CT image analysis

Lung parenchymal volume (L) (in cm^3) excluding large and small pulmonary vessels, macroscopic emphysematous airspace volume (E) (in cm^3) based on a -910HU threshold mask, fraction of lung emphysema (F=E/L), and mean attenuation of non-emphysematous lung parenchyma (A) (in HU) were calculated from CT images using the image analysis software system 3DVIEWNIX. The following three steps were implemented during the segmentation process.

First, each lung was segmented via a fuzzy connectedness (FC) algorithm [8, 9]. This algorithm is a measure of the strength of connection between voxels in a given image, where the strength between any two voxels c and d in the image is determined by considering all connecting paths (where each path is a sequence of adjacent voxels) between c and d, by assigning a strength of connection to each such path, and by taking the maximum of all strengths. The strength assigned to a path is the smallest "affinity" between each pair of voxels along the path, where the affinity between two adjacent voxels u and v along a path is determined based on the image intensity difference between u and v and the actual image intensities at u and v. The parameters of the affinity function were estimated from the image intensities within a few sample lung regions that were painted interactively on a few image slices by the operator. Once estimated, the parameters were fixed for all datasets analyzed in this study. The only other input required for the FC algorithm were the initial seed voxels in the left and right lungs with locations close to the points (X/4, Y/2, Z/2) and (3X/4, Y/2, Z/2), where X, Y, Z are the width, depth, and the height of the imaged body region (all in mm). Second, within the segmented lungs, all voxels with attenuation of ≥-600HU were considered to constitute pulmonary vessels and were removed from the lung masks. Third, within each remaining lung mask region, all voxels with attenuation ≤-910HU were considered to constitute emphysematous lung. Once delineated, the volumetric and attenuation parameters specified above were computed (Fig. 1 and 2).

PET image analysis

Lung uncorrected maximum SUV (USUVmax) was measured manually from PET images on two dedicated workstations (PETView, Philips Healthcare, Best, The Netherlands for the analysis of PET datasets from ^{18}F-FDG-PET scans, and Extended Brilliance Workstation, Philips Healthcare, Best, The Netherlands for the analysis of PET datasets from ^{18}F-FDG-PET/CT scans). Two circular regions of interest (ROI) ~2cm in diameter were manually placed in the periphery of each lung in locations where no pulmonary abnormality other than emphysema (when present) was seen on corresponding CT images, while simultaneously avoiding overlap with visible locations of large pulmonary vessels and bronchi. One ROI was placed at the craniocaudal midlevel of the upper half of the lung and the other at the craniocaudal midlevel of the lower half of the lung, such that the average of the two USUVmax measurements was taken as the overall USUVmax of the lung.

A first level of partial volume correction (PVC) of lung USUVmax to account for the presence and degree of macroscopic emphysematous air space was calculated as CSUVmax=USUVmax/(1-F), since 1-F represents the fraction of non-emphysematous lung within the entire lung. A second level of PVC of non-emphysematous lung CSUVmax to account for the mixture of air and lung parenchyma at the microscopic level was then calculated as CCSUVmax=CSUVmax/k where k=(A+1000/1040). Please note that k, the fraction of lung parenchymal tissue within the non-emphysematous lung, was derived from the following equation: non-emphysematous lung parenchyma attenuation (A)=k*(gasless lung

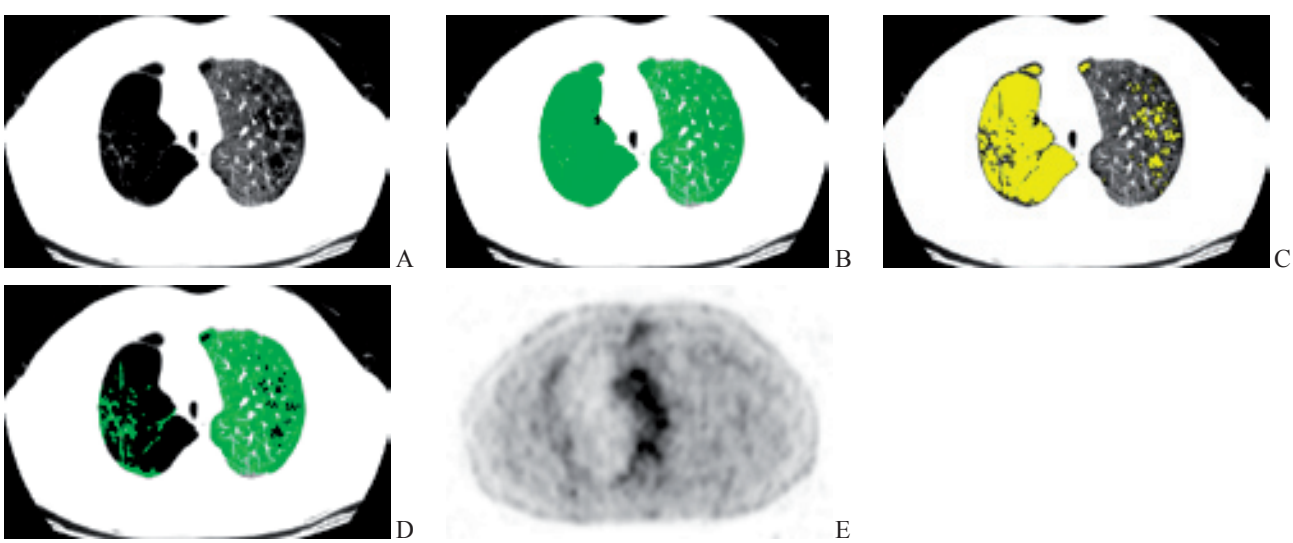

Figure 2. A 60 years old man with centrilobular emphysema. A. Axial chest CT image reveals moderate centrilobular emphysema in left upper lung zone and severe centrilobular emphysema in right upper lung zone. B. Same axial chest CT image with color overlay demonstrates bilateral lung segmentation with exclusion of pulmonary vessels. C. Same axial chest CT image with new color overlay highlights voxels with attenuation ≤ -910HU in lungs considered as emphysematous. D. Same axial chest CT image with new color overlay shows remaining voxels in lungs considered as non-emphysematous. E. Corresponding axial ^{18}F-FDG-PET image through upper lung zones. Note apparently decreased ^{18}F-FDG uptake in right lung compared to that of left lung due to dilutional effect of more severe emphysema on right, which emphasizes the necessity for partial volume correction to accurately quantify lung inflammation.

parenchyma attenuation)+(1 - k)*(air attenuation), where we assumed that air attenuation =-1000HU and gasless lung parenchyma attenuation is 40HU.

The effect of PVC upon SUV measurements was assessed via calculation of percent change between CSUVmax and USUVmax (%UC), and of percent change between CCSUVmax and USUVmax (%UCC).

Statistical analysis

Tabulations of means, standard deviations, and ranges of variables were performed, where each lung per subject was treated as contributing its own set of data points. Linear regression analyses between USUVmax, CSUVmax, CCSUVmax, %UC, and %UCC as dependent variables and F as the independent variable were subsequently performed.

All data acquired from quantitative analysis were recorded in a computerized spreadsheet (Microsoft Excel 2007; Microsoft, Redmond, WA). All statistical analyses were performed using Stata software (Stata/IC Version 10.1, StataCorp, College Station, TX). P values <0.05 were considered as indicating statistical significance.

Results

Mean lung parenchymal volume (L) was 2225.89±729.04cm^3 (range 24.02-3716.86cm^3), mean emphysema volume (E) was 289.75±379.26cm^3 (range 0.00-1727.12cm^3), and mean fraction of lung emphysema (F) was 0.12±0.15 (range: 0.00-0.70). The average mean attenuation of non-emphysematous lung parenchyma (A) was -829.49±27.14HU (range –752–-868HU). Mean USUVmax was 0.57±0.23 (range 0.15-1.50), mean CSUVmax was 0.68±0.41 (range 0.18-3.64), and mean CCSUVmax was 4.29±3.16 (range 1.14-28.71). Mean %UC was 19.04±33.99% (range 0.00-228.48%) and mean %UCC was 648.43±292.79% (range 320.13-2221.59%).

USUVmax was not significantly correlated with F (r=-.0973, P=0.34), whereas CSUVmax (r=0.4660, P<0.0001) and CCSUVmax (r=0.5479, P<0.0001) were significantly positively correlated with F (Fig. 3). As per the relationship between the random variables F and CSUVmax and CCSUVmax, positivity of the correlation is to be expected. Linear regression equations between these variables were as follows: USUVmax=-0.147*F+0.589, CSUVmax=1.274*F+0.529, and CCSUVmax=11.606*F+2.891. %UC (r=0.9383, P<0.0001) and %UCC (r=0.9369, P<0.0001) were significantly positively correlated with F (Fig. 4). Associated linear regression equations were as follows: %UC=213.45%*F-6.65% and %UCC=1835.82%*F + 427.48%.

Discussion

Although inhalation of toxic gases and particles, such as from tobacco use, are major risk factors for COPD, induced inflammation plays a key role in its pathogenesis [10, 11]. This inflammatory process involves a complex interplay between lung epithelial cells, endothelial cells, and fibroblasts with

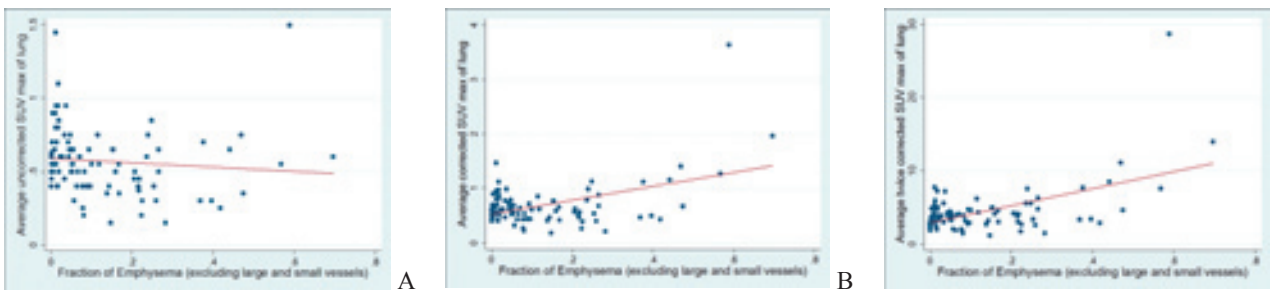

Figure 3. Scatterplots and linear regression demonstrating relationship of pulmonary metabolism measured from ^{18}F-FDG-PET to severity of lung emphysema measured from diagnostic CT. A. Average lung uncorrected maximum SUV (USUVmax) vs. mean fraction of lung emphysema (F). USUVmax is not significantly correlated with F (r=-.0973, P=0.34, linear regression equation USUVmax=-0.147*F+0.589). B. Average lung USUVmax partial volume corrected to account for presence of macroscopic emphysema (CSUVmax) vs. mean fraction of lung emphysema (F). CSUVmax is significantly positively correlated with F (r=0.4660, P<0.0001, linear regression equation CSUVmax=1.274*F+0.529). C. Average lung CSUVmax partial volume corrected to account for mixture of air and lung parenchyma at microscopic level (CCSUVmax) vs. mean fraction of lung emphysema (F). CCSUVmax is significantly positively correlated with F (r=0.5479, P<0.0001, linear regression equation CCSUVmax=11.606*F+2.891). Note variability of lung metabolism amongst subjects with similar amounts of emphysema.

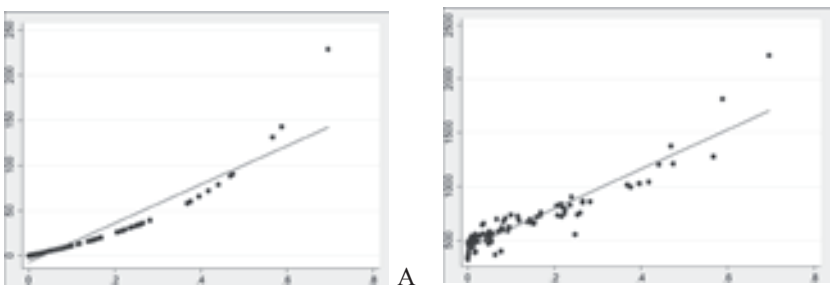

Figure 4. Quantitative effects of partial volume correction upon average lung SUV measurements to account for presence and degree of macroscopic emphysema as well as mixture of air and lung parenchyma at microscopic level. A. Percent change from USUVmax to CSUVmax (%UC) vs. mean fraction of lung emphysema (F). %UC is significantly positively correlated with F (r=0.9383, P<0.0001, linear regression equation %UC=213.45%*F - 6.65%). B. Percent change from USUVmax to CCSUVmax (%UCC) vs. mean fraction of lung emphysema (F). %UCC is significantly positively correlated with F (r=0.9369, P<0.0001, linear regression equation %UCC=1835.82%*F+427.48%).

infiltrating neutrophils, macrophages, eosinophils, and subpopulations of both CD4+ and CD8+T cells, and is associated with induced chronic oxidative stress and protease-anti-protease imbalance, which are also involved in COPD pathogenesis [12-14]. Patients with greater degrees of emphysema on CT have been reported to have more continuous inflammation based on elevated sputum neutrophil count, elevated lung neutrophils, and the relationship of tissue neutrophil elastase distribution with emphysema [15, 16]. These findings support the hypothesis that immune responses contribute to the pathology of COPD, where exacerbations and progression of COPD may be a manifestation of the vicious cycle of infection and inflammation with associated tissue destruction, although the etiological factors involved are not fully understood [10, 17, 18].

Current approaches beyond clinical assessment used to assess patients with COPD include pulmonary function testing (PFT), laboratory testing, as well as structural imaging and gross functional imaging techniques such as computed tomography (CT) and hyperpolarized gas magnetic resonance imaging (MRI), although they all have limitations. For example, PFT is easy to perform and is reproducible, but only provides indirect global functional measures of the status of the lungs and airways, is insensitive for early subclinical disease, and is limited for purposes of prognosticating outcome, guiding therapy, or monitoring disease activity given the heterogeneity of COPD [4, 5]. Similarly, laboratory testing for markers of inflammation such as plasma fibrinogen and C-reactive protein is easy to perform and may be useful to identify presence of COPD and to improve patient outcome prediction, but provides only indirect global measures of inflammatory disease that are not specific for COPD and may not predict lung function decline [19].

Computed tomography provides detailed structural information and limited functional information about the amount and distribution of airspace and airways disease, and is therefore useful for phenotyping COPD as emphysema predominant, airways predominant, or mixed. However, it provides no information about the underlying molecular pathophysiological processes that are present, and may be prone to variability due to differences in imaging technique [20-22]. Hyperpolarized gas MRI also provides structural and functional information about the lungs and airways and does not involve the use of ionizing radiation, but similarly does not provide molecular information which may be relevant for purposes of phenotyping, pretreatment planning, and prediction of outcome. Furthermore, it is not widely available in community centers, is technically challenging to implement, and is also prone to variability due to differences in imaging technique [23, 24]. As such, there is still a need for non-invasive techniques to provide molecular information about the status of the lungs and airways in patients with COPD.

Fluorine-18-FDG-PET has increasingly been utilized to quantify pulmonary and airways inflammation in both animal studies and human studies. Activated inflammatory cells, particularly neutrophils, increase glucose metabolism to much greater levels than non-neoplastic lung tissue, and therefore are detectable and quantifiable on ^{18}F-FDG-PET images [25-28]. In particular, the significant increase in pulmonary ^{18}F-FDG uptake observed in the setting of acute lung injury is reported to be mainly due to neutrophil sequestration and activation in the lungs rather than due to accumulation of ^{18}F-FDG in edema fluid secondary to increased pulmonary vascular permeability [25].

Only a few studies in the literature have reported the application of ^{18}F-FDG-PET in the setting of COPD. Jones et al (2003) reported that the mean ^{18}F-FDG uptake in the lungs measured through PET imaging was significantly higher in 6 patients with COPD compared to that of 6 patients with asthma (a 235% increase) and 6 normal controls (a 266% increase), although sputum neutrophils and eosinophils were increased in both COPD and asthma patient groups [29]. They attributed these observations to a marked difference in the nature of the inflammatory response between patients with COPD and asthma, most likely due to increased pulmonary localization and metabolic activation of neutrophils in COPD patients [12, 26-29]. In this study, lung glucose metabolic activity was calculated as the slope of a Patlak plot constructed from tissue:plasma radioactivity measurements from lung regions of interest and venous blood radioactivity measurements, and then corrected for the initial tissue distribution volume of ^{18}F-FDG obtained from the plot intercept [29]. Several other investigators have reported increased ^{18}F-FDG uptake in thoracic and abdominal muscles as well as in the right heart in patients with COPD [30-33]. Coulson et al (2010) recently reported that COPD patients exhibit aortic inflammation that is detectable as increased aortic ^{18}F-FDG uptake on ^{18}F-FDG-PET/CT imaging [34].

To our knowledge, our study is the first in the literature to assess the effects of partial volume correction upon SUV measurements of pulmonary parenchymal inflammation obtained from ^{18}F-FDG-PET/CT in relation to varying amounts of emphysema, although we had previously reported the methodology and preliminary results of this approach in 2009 [35]. The only other study in the literature using this approach was conducted by Lambrou et al (2011), where they similarly applied the second level of partial volume correction at the voxel level based on the low dose attenuation CT images acquired during ^{18}F-FDG-PET/CT in 5 patients with diffuse parenchymal lung disease and 12 patients with normal lungs [36].

Partial volume correction is important since measurement of lesion SUV is susceptible to the partial volume effect due to image blurring and image sampling. As such, this effect generally leads to underestimation of metabolic activity of focal lesions with size $\leq$2-3 times full-width-at-half-maximum (FWHM) of the reconstructed image resolution [37-40]. Similarly, for purposes of lung parenchymal assessment, the partial volume effect leads to underestimation of lung parenchymal SUV due to the mixture of metabolically active lung parenchymal tissue and non-metabolically active air space components (whether from presence of macroscopic emphysema or from presence of air within the alveolar air spaces and distal airways at the microscopic level within aerated lung), and is accentuated with increasing amounts of emphysema. Unfortunately, partial volume correction of SUV measurements is currently not performed in routine clinical practice, leading to significant errors in disease quantification.

Lambrou et al (2011) reported that on average, partial volume corrected SUV of lung was increased by 281% compared to the uncorrected SUV ($P<0.001$) [36]. In our study, we demonstrated that a first level of partial volume correction of SUVmax to account for the presence of macroscopic emphysematous air space led to an average increase of 19%

in lung SUVmax, and that a second level of partial volume correction of SUVmax to account for the mixture of air and lung parenchyma at the microscopic level led to an average increase of 648% in lung SUVmax. Importantly, we observed a significant correlation between lung metabolism and the degree of emphysema only when partial volume correction was implemented. Interestingly, it is apparent from the graphs of lung SUV versus fraction of emphysema that there is variability of lung SUV amongst subjects who have similar amounts of emphysema. This suggests that ^{18}F-FDG-PET may provide unique molecular information that is synergistic with other non-molecular imaging modalities to predict outcome and delineate phenotype in patients with COPD, although further research will be required to validate this hypothesis.

This study has several limitations. First, it was performed retrospectively utilizing a relatively small cross-sectional sample of subjects, potentially leading to selection and other unknown biases. In particular, we did not account for potentially confounding variables related to current or former smoker status, amount of tobacco use, gender, body mass index, or presence of other comorbidities. Second, no reference standards for assessment of pulmonary inflammation using non-imaging based methodologies were available for validation purposes. Moreover, it is likely that some of the measured signal from ^{18}F-FDG in the lung on PET images was contributed by ^{18}F-FDG within the pulmonary vasculature rather than due to cellular uptake of ^{18}F-FDG in the lung parenchyma. Third, PET image acquisition was performed on different PET only or PET/CT instruments during quiet respiration, and diagnostic CT image acquisition was performed on several different CT scanners during full inspiration, potentially leading to data variability as well as systematic overestimation of second level partial volume correction of lung SUV measurements due to differences in inspiration. In addition, the time interval between ^{18}F-FDG-PET and diagnostic CT acquisitions was on average 39 days long, which is suboptimal. Fourth, PET image analysis was performed on a region of interest basis to obtain average global lung SUV measurements, and diagnostic CT image analysis parameters were used to apply partial volume correction uniformly to global lung SUV measurements rather than on a voxel by voxel basis. As such, details regarding the spatial variability of voxel level pulmonary parenchymal metabolism in relation to the amount and spatial distribution of emphysema within the lung were not obtained. Fifth, it was not possible to separate very small pulmonary vessels from non-vascular pulmonary parenchyma during pulmonary segmentation on diagnostic CT, and simple assumptions were made regarding the attenuation properties of gasless lung parenchyma and pure air, potentially leading to errors in partial volume correction. Despite these limitations, we observed statistically significant results through use of an easy to implement quantitative approach that are concordant with reports in the non-imaging literature regarding the key role of inflammation in the pathogenesis of emphysema.

Future studies will need to be performed to further examine the observations made in this preliminary study on a larger scale in a prospective manner to address some of these limitations. We note that, from the knowledge of the boundaries of the emphysematous region and the pattern of voxels around each voxel in these boundaries, it may be possible to estimate the partial volume effect and perform partial volume correction more accurately than with the more global method we have presented in this manuscript. This direction will be considered in future studies.

In conclusion, ^{18}F-FDG-PET is useful to non-invasively detect and quantify pulmonary inflammation in patients with COPD. In particular, we have shown that pulmonary inflammation measured on ^{18}F-FDG-PET is significantly positively correlated with emphysema severity in vivo, and that this correlation is observed only when partial volume correction is implemented to account for the dilutional effects of pulmonary air upon lung parenchymal SUV measurements. These findings support the notion that pulmonary inflammation is a key contributor to the development and progression of emphysema. Future larger scale prospective studies will need to be performed to assess the potential utility of this approach to individually phenotype disease, plan treatment, predict disease progression, prognosticate patient outcome, and quantify response assessment in the setting of COPD.

The authors declare that they have no conflicts of interest.

Bibliography

1. Mathers CD, Loncar D. Projections of global mortality and burden of disease from 2002 to 2030. *PLoS Med* 2006; 3: e442. doi:10.1371/journal.pmed.0030442.
2. Morbidity & Mortality: *2012 Chart Book on Cardiovascular, Lung, and Blood Diseases*. Available at: http://www.nhlbi.nih.gov/resources/docs/cht-book.htm Accessed 7/4/2012: National Institutes of Health, National Heart, Lung, and Blood Institute (NHLBI); 2012.
3. Minino AM. Death in the United States, 2009. *NCHS data brief* 2011: 1-8.
4. Rosenberg SR, Kalhan R. Biomarkers in chronic obstructive pulmonary disease. Translational research. *J Lab Clin Med* 2012; 159: 228-37. doi:10.1016/j.trsl.2012.01.019.
5. Vestbo J, Rennard S. Chronic obstructive pulmonary disease biomarker(s) for disease activity needed--urgently. *Am J Respir Crit Care Med* 2010; 182: 863-4. doi:10.1164/rccm.201004-0602ED.
6. Han MK, Agusti A, Calverley PM et al. Chronic obstructive pulmonary disease phenotypes: the future of COPD. *Am J Respir Crit Care Med* 2010; 182: 598-604. doi:10.1164/rccm.200912-1843CC.
7. Schuster DP. The opportunities and challenges of developing imaging biomarkers to study lung function and disease. *Am J Respir Crit Care Med* 2007; 176: 224-30.
8. Udupa JK, Samarasekera S. Fuzzy connectedness and object definition: Theory, algorithms, and applications in image segmentation. *Graph Model Im Proc* 1996; 58: 246-61.
9. Udupa JK, Saha PK. Fuzzy connectedness in image segmentation. *Proc IEEE Inst Electr Electron Eng* 2003; 91: 1649-69.
10. van Eeden SF, Hogg JC. Chronic obstructive pulmonary disease: do regional differences in tissue inflammation matter? *Respiration* 2011; 81: 359-61. doi:10.1159/000323869.
11. Roth M. Pathogenesis of COPD. Part III. Inflammation in COPD. *Int J Tuberc Lung Dis* 2008; 12: 375-80.
12. Finkelstein R, Fraser RS, Ghezzo H, Cosio MG. Alveolar inflammation and its relation to emphysema in smokers. *Am J Respir Crit Care Med* 1995; 152: 1666-72.
13. Tetley TD. Inflammatory cells and chronic obstructive pulmonary disease. *Curr Drug Targets Inflamm Allergy* 2005; 4: 607-18.

14. Fischer BM, Pavlisko E, Voynow JA. Pathogenic triad in COPD: oxidative stress, protease-antiprotease imbalance, and inflammation. *Int J Chron Obstruct Pulmon Dis* 2011; 6: 413-21. doi:10.2147/copd.s10770.
15. Hunninghake GW, Crystal RG. Cigarette smoking and lung destruction. Accumulation of neutrophils in the lungs of cigarette smokers. *Am Rev Respir Dis* 1983; 128: 833-8.
16. Braber S, Thio M, Blokhuis BR et al. An association between neutrophils and immunoglobulin free light chains in the pathogenesis of chronic obstructive pulmonary disease. *Am J Respir Crit Care Med* 2012; 185: 817-24. doi:10.1164/rccm.201104-0761OC.
17. Sze MA, Dimitriu PA, Hayashi S et al. The lung tissue microbiome in chronic obstructive pulmonary disease. *Am J Respir Crit Care Med* 2012; 185: 1073-80. doi:10.1164/rccm.201111-2075OC.
18. Hurst JR, Vestbo J, Anzueto A et al. Susceptibility to exacerbation in chronic obstructive pulmonary disease. *N Engl J Med* 2010; 363: 1128-38. doi:10.1056/NEJMoa0909883.
19. Shaker SB, von Wachenfeldt KA, Larsson S et al. Identification of patients with chronic obstructive pulmonary disease (COPD) by measurement of plasma biomarkers. *The clinical respiratory journal* 2008; 2: 17-25. doi:10.1111/j.1752-699X.2007.00032.x.
20. Diaz AA, Come CE, Ross JC et al. Association between airway caliber changes with lung inflation and emphysema assessed by volumetric CT scan in subjects with COPD. *Chest* 2012; 141: 736-44. doi:10.1378/chest.11-1026.
21. Madani A, Van Muylem A, Gevenois PA. Pulmonary emphysema: effect of lung volume on objective quantification at thin-section CT. *Radiology* 2010; 257: 260-8. doi:10.1148/radiol.10091446.
22. Gierada DS, Bierhals AJ, Choong CK et al. Effects of CT section thickness and reconstruction kernel on emphysema quantification relationship to the magnitude of the CT emphysema index. *Acad Radiol* 2010; 17: 146-56. doi:10.1016/j.acra.2009.08.007.
23. Quirk JD, Lutey BA, Gierada DS et al. In vivo detection of acinar microstructural changes in early emphysema with (3)He lung morphometry. *Radiology* 2011; 260: 866-74. doi:10.1148/radiol.11102226.
24. Peterson ET, Dai J, Holmes JH, Fain SB. Measurement of lung airways in three dimensions using hyperpolarized helium-3 MRI. *Phys Med Biol* 2011; 56: 3107-22. doi:10.1088/0031-9155/56/10/014.
25. Chen DL, Schuster DP. Positron emission tomography with [18F]fluorodeoxyglucose to evaluate neutrophil kinetics during acute lung injury. *Am J Physiol Lung Cell Mol Physiol* 2004; 286: L834-40. doi:10.1152/ajplung.00339.2003.
26. Jones HA, Cadwallader KA, White JF et al. Dissociation between respiratory burst activity and deoxyglucose uptake in human neutrophil granulocytes: implications for interpretation of ^{18}F-FDG PET images. *J Nucl Med* 2002; 43: 652-7.
27. Jones HA, Schofield JB, Krausz T et al. Pulmonary fibrosis correlates with duration of tissue neutrophil activation. *Am J Respir Crit Care Med* 1998; 158: 620-8.
28. Jones HA, Clark RJ, Rhodes CG et al. In vivo measurement of neutrophil activity in experimental lung inflammation. *Am J Respir Crit Care Med* 1994; 149: 1635-9.
29. Jones HA, Marino PS, Shakur BH, Morrell NW. In vivo assessment of lung inflammatory cell activity in patients with COPD and asthma. *Eur Respir J* 2003; 21: 567-73.
30. Osman MM, Tran IT, Muzaffar R et al. Does ^{18}F-FDG uptake by respiratory muscles on PET/CT correlate with chronic obstructive pulmonary disease? *J Nucl Med Technol* 2011; 39: 252-7. doi:10.2967/jnmt.111.089961.
31. Basu S, Alzeair S, Li G et al. Etiopathologies associated with intercostal muscle hypermetabolism and prominent right ventricle visualization on 2-deoxy-2[F-18]fluoro-D-glucose-positron emission tomography: significance of an incidental finding and in the setting of a known pulmonary disease. *Mol Imaging Biol* 2007; 9: 333-9. doi:10.1007/s11307-007-0102-7.
32. Aydin A, Hickeson M, Yu JQ et al. Demonstration of excessive metabolic activity of thoracic and abdominal muscles on FDG-PET in patients with chronic obstructive pulmonary disease. *Clin Nucl Med* 2005; 30: 159-64.
33. Duarte PS, Zhuang H, Machado C et al. Increased FDG uptake in the right cardiac chambers in a patient with pulmonary emphysema. *Clin Nucl Med* 2002; 27: 605-6.
34. Coulson JM, Rudd JH, Duckers JM et al. Excessive aortic inflammation in chronic obstructive pulmonary disease: an ^{18}F-FDG PET pilot study. *J Nucl Med* 2010; 51: 1357-60. doi:10.2967/jnumed.110.075903.
35. Dam V, Chen X, Alavi A et al. Novel quantitative measurement of pulmonary inflammation in COPD by FDG PET and CT segmentation. *J Nucl Med* 2009; 50: 1397.
36. Lambrou T, Groves AM, Erlandsson K et al. The importance of correction for tissue fraction effects in lung PET: preliminary findings. *Eur J Nucl Med Mol Imaging* 2011; 38: 2238-46. doi:10.1007/s00259-011-1906-x.
37. Hickeson M, Yun M, Matthies A et al. Use of a corrected standardized uptake value based on the lesion size on CT permits accurate characterization of lung nodules on FDG-PET. *Eur J Nucl Med Mol Imaging* 2002; 29: 1639-47.
38. Chawluk JB, Alavi A, Dann R et al. Positron emission tomography in aging and dementia: effect of cerebral atrophy. *J Nucl Med* 1987; 28: 431-7.
39. Soret M, Bacharach SL, Buvat I. Partial-volume effect in PET tumor imaging. *J Nucl Med* 2007; 48: 932-45.
40. Basu S, Zaidi H, Houseni M et al. Novel quantitative techniques for assessing regional and global function and structure based on modern imaging modalities: Implications for normal variation, aging and diseased states. *Sem Nucl Med* 2007; 37: 223-39.